Intravascular Magnetic Resonance Imaging Using a Loopless Catheter Antenna

Ogan Ocali, Ergin Atalar

Recently, intravascular catheter probes have been developed to increase signal-to-noise ratio (SNR) for MR imaging of blood vessels. Miniaturization of these catheter probes without degrading their performances is very critical in imaging small vessels such as coronary arteries. Catheter coils have a loop incorporated in their structure and have limitations in physical dimensions and electromagnetic properties. The use of a loopless intravascular catheter antenna is proposed to overcome these problems. The catheter antenna is essentially a dipole, which makes a very thin diameter possible, and its electronic circuitry can be placed outside the blood vessels without performance degradation. The theoretical foundation for the design and operation of the catheter antenna is presented. Several catheter antennae, as small as 1.5 French, were constructed and tested on phantoms and rabbits with great success. The catheter antenna has a simple structure and is easy to design, implement, and operate.

Key words: Intravascular MRI; MR catheter coil; atherosclerosis; MRI of arterial wall.

INTRODUCTION

In the detection of atherosclerotic disease, the precision and accuracy of current methods to characterize plaques and monitor therapy are inadequate. Angiography displays the vessel lumen, but the vessel wall cannot be visualized nor can atherosclerotic plaques be characterized. In a limited number of applications, intravascular ultrasound (1) is being used to acquire images of atherosclerotic plaques. The quality of the resulting images, however, is not satisfactory (2). Furthermore, interpretation of ultrasound images is not easy and requires a significant amount of experience.

With MR techniques, however, it is possible to distinguish between the three layers of the vessel wall and detect atherosclerotic lesions, even before they calcify (3–6). In addition, MR images are much easier to interpret and provide precise information about the biochemical structure of the vessel wall and the plaques, which is critical in understanding the disease. However, the signal-to-noise ratio (SNR) that is obtained with standard receiver coils is not sufficiently high for the desired resolution.

To achieve satisfactory image quality, a small receiver probe can be placed inside blood vessels. The first catheter coil was built by Kantor *et al.* in 1983 to increase SNR in phosphorus MR spectra of the heart (7). Recently, catheter coils have been designed for imaging the arterial wall (8–11). These catheter coil designs, however, are mechanically too rigid and large to image small vessels. As a solution to this problem, imaging the arterial wall with an expandable coil placed in a nearby vein also has been proposed (12).

Recently, we presented an alternative catheter coil design (13). These coils are formed by short-circuiting one end of a two-conductor transmission line, which allows smaller size and greater flexibility than previous designs. This design was tested on various phantoms, animals, and isolated human aortas. Both the signal and noise received by these catheter coils are very small. Hence, the noise that is generated by the cable connecting the catheter coil to the tuning and matching circuit may reduce SNR significantly. Therefore, the tuning and matching circuits must be placed very close to the catheter coil, inside the blood vessels. This imposes a size restriction on the circuits. Currently, tuning and matching circuits that are about 3 mm in diameter can be constructed, using off-the-shelf standard microwave monolithic integrated circuit components.

In this paper, we describe a novel intravascular catheter antenna design. The catheter antenna is essentially a wire and, therefore, can be made very thin. Moreover, its electromagnetic properties are virtually independent of its diameter, unlike coils that incorporate a loop. Both the noise and signal power acquired by this antenna are very high, which allows the tuning and matching circuits to be placed outside blood vessels. Its small size makes it possible to insert the catheter antenna into very-small-diameter blood vessels. Because the catheter antenna has an extremely high sensitivity and SNR in its immediate vicinity, it can provide near-microscopic resolution, in addition to the advantageous tissue characterization of MRI.

THEORY

The catheter antenna contains a dipole antenna portion. A piece of conducting wire serves as one of the poles. The second pole is constructed over the outer surface of a thin coaxial cable that carries the MR signal to the matching, tuning, and decoupling circuit. The whole dipole antenna and part of the coaxial cable are inserted into the blood vessels.

To estimate the performance of the catheter antenna and compare it with catheter coils, we established the operational theory for the catheter antenna. The theoretical foundation for the catheter antenna design and analysis is developed in this section.

MRM 37:112–118 (1997)

From the Johns Hopkins University School of Medicine, Department of Radiology, Baltimore, Maryland.

Address correspondence to: Ergin Atalar, Ph.D., Department of Radiology, Johns Hopkins University School of Medicine, 601 North Caroline Street JHOC 4241, Baltimore, MD 21287-0845.

Received February 2, 1996; revised July 1, 1996; accepted July 2, 1996.

This work was supported by the Whitaker Foundation.

0740-3194/97 $3.00

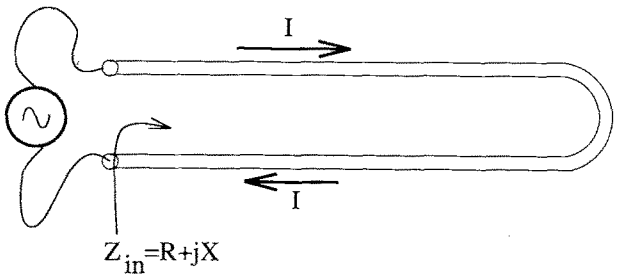

FIG. 1. Catheter coil ($R \approx 0.5\ \Omega$).

Catheter Antenna

Using the reciprocity principle (14), the signal voltage in an MRI experiment is given as:

$$V_S = \omega\mu HM \qquad [1]$$

where V_S is the signal voltage, M is the transverse magnetization of the voxel, and H is the magnetic field generated by the coil in the transverse plane for unit input current. Of the factors affecting the signal voltage, H is the only coil-dependent parameter.

The root-mean-square (RMS) noise voltage can be calculated as:

$$V_N = \sqrt{4k_B T R f_e} \qquad [2]$$

where k_B is the Boltzmann constant, T is the sample temperature, f_e is the effective pixel bandwidth, and R is the real part of the input impedance seen from the input terminals of the coil. The effective pixel bandwidth is computed as:

$$f_e = \frac{2BW}{N_x N_y NEX} \qquad [3]$$

where NEX is the number of image repetitions, N_x and N_y are the number of readout points and phase-encoding steps, respectively, and BW is the receiver bandwidth. Observe that this expression accounts for the noise reduction due to effective data averaging that is performed during image construction.

The only coil-dependent parameter that affects the noise voltage is R. Combining Eqs. [1] and [2], SNR is given as:

$$\mathrm{SNR} = \frac{V_S}{V_N} \propto \frac{H}{\sqrt{R}} \qquad [4]$$

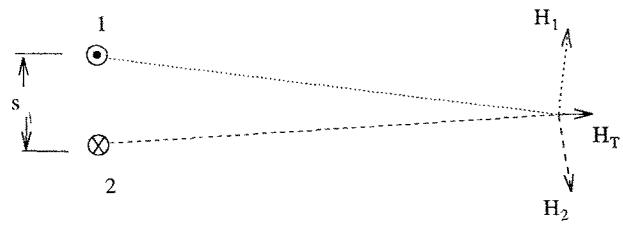

FIG. 2. Field cancellation in a catheter coil, axial view. H_1 and H_2 are proportional to $1/r$, and the total field, H_T, is proportional to s/r^2.

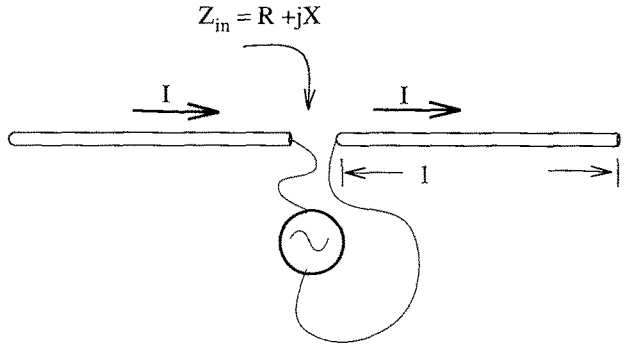

FIG. 3. Catheter antenna; arrows indicate the current flow. The current path is not completed. The current periodically charges the poles in reverse polarities.

To improve SNR we must increase H and decrease R, which usually are conflicting goals. In the catheter coil structure proposed by Atalar *et al.* (13), which incorporates a loop (Fig. 1), magnetic fields generated by the two conductors partially cancel each other, and this cancellation effect becomes more pronounced as the distance from the coil increases, as seen in Fig. 2. The performance of the coil, therefore, depends strongly on the separation of the conductors.

Cancellation of the fields can be avoided by separating the conductors as seen in Fig. 3. The coil mutates into a dipole antenna as a result. Obviously, the H field increases considerably with this operation. In this configuration, the current path is not completed and charges simply oscillate between the two tips of the antenna. Some resistive current will flow through the surrounding medium due to the nonzero conductance of the medium. The noise resistance, R, increases considerably because of the increase in stray electric field losses.

The sensitivity profile of the catheter antenna depends on its orientation with respect to the main field, similar to surface or catheter coils. Only the transverse component of the H field that is generated by the catheter antenna contributes to the signal. Therefore, the best performance is achieved when the catheter antenna is aligned parallel to the main magnetic field.

A sample design for the catheter antenna is given in Fig. 4. The inner conductor and the secondary shield act as poles of the dipole antenna. The dielectric coating under the secondary shield acts as a balancing transformer, which disables current flow on the outer surface of the primary shield.

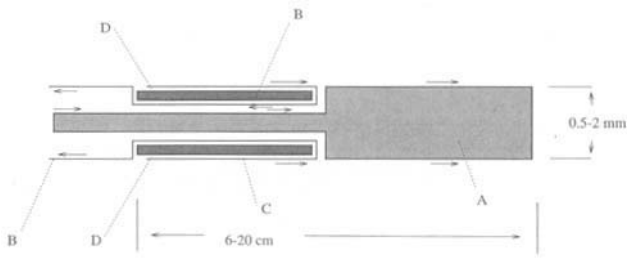

FIG. 4. Sectional view of the catheter antenna. A, inner conductor; B, primary shield; C, secondary shield; D, high ϵ_r insulator. Arrows indicate current-carrying surfaces of the conductors.

The unbalanced currents distort the fields and make the input impedance of the antenna sensitive to changes in loading conditions and position of the antenna and the coaxial cable. The magnetic field that is generated by these currents may also interfere with the RF excitation field and create a nonuniform flip angle. For optimal balancing, the dielectric constant of the insulator between the primary and the secondary conductors must be chosen such that the transmission line formed by the primary and the secondary shields has a length of $\lambda/4$. This greatly reduces the unbalanced current flowing on the outer surface of the primary shield.

It is also possible to construct a catheter antenna without the secondary shield, which makes the design more susceptible to unbalancing effects. Fortunately, the high loss of the medium causes the unbalanced currents on the outer surface of the primary shield to decay exponentially along the length of the cable, making the effects tolerable. Without the secondary shield, the whole length of the coaxial cable is able to pick up MR signal, which may be a desirable effect for certain cases such as active catheter tracking under MR fluoroscopy.

The catheter antenna supplies a high signal voltage, because there are no field cancellations as in a catheter coil. To obtain a theoretical estimate of the SNR performance of the design, the noise resistance, R, which is the real part of the antenna impedance, must be calculated. To estimate the antenna impedance, we solved the associated electromagnetic problem.

Computation of the Antenna Impedance and the H Field

The Carson formulation for a dipole antenna is (15):

$$Z_{in} = \int_{-l}^{l} I(z)^* E(z) dz \qquad [5]$$

where z is the distance from the center of the antenna, $E(z)$ is the electric field, $I(z)$ is the current, and * denotes complex conjugation.

We approximate the current distribution by a generalization of the cosine current distribution for lossless antennae given in ref. 15:

$$I(z) = \frac{e^{-jkz} - e^{-jkz}(e^{-2jk(l-z)})}{1 - e^{-2jkl}} \qquad [6]$$

where l is the length of each pole and k is the complex propagation constant,

$$k = (k_1 - jk_2) = \frac{1}{j}\sqrt{\mu(-\omega^2\epsilon + j\omega\sigma)} \qquad [7]$$

where we set $\mu = \mu_0$, the permeability of free space. For the dielectric constant, ϵ, and conductivity, σ, we use values representative of human tissue at 50–200 MHz (16): $\epsilon = \epsilon_r\epsilon_0$, where $\epsilon_r \approx 75$ and $\sigma \approx 0.8$ Siemens/meter.

Observe that this current distribution consists of two current waves, one propagating from the terminal to the tip and the other propagating backward from the tip, and the propagation constant is the same as the surrounding medium. This is equivalent to approximating the dipole antenna by a biconical transmission line, which is commonly used for dipole antenna computations. Also note that the current is zero at the tip and unity at the terminal of the antenna.

From electromagnetic theory, it is known that (15):

$$E = -j\omega\left\{A + \frac{1}{k^2}\nabla^2 A\right\} \qquad [8]$$

where A is the vector potential and ∇^2 denotes the Laplacian operator. In terms of differential current segments, the vector potential is given as:

$$A = \int \mu \frac{I(z')e^{-jkd(z')}}{4\pi d(z')} dz' \qquad [9]$$

where $d(z')$ denotes the distance between the current element and the observation point.

Using Eqs. [8] and [9] in Eq. [5] we obtain:

$$Z_{in} = \int_{-l}^{l}\int_{-l}^{l} I(z)^* I(z') G(z, z') dz dz' \qquad [10]$$

where $G(z, z')$ gives approximately the vertical component of the electric field at z and at distance t (radius of the conductor) from the center of the conductor due to the current at z' passing from the center of the conductor (see Fig. 5). We approximate the effect of the current flowing on the surface of the conductor by a filamentary current passing from the center of the conductor, a value 2π times the surface current on the conductor. We also assume that the conductor losses are negligible.

Under these assumptions, we find $G(z, z')$ after symbolic manipulation using Mathematica software (Wolfram Research Inc, Champaign, IL), as

$$G(z, z') = \frac{j\omega\mu_0 e^{-jkd}}{4\pi} \left[\frac{1}{d} + \frac{3jk(z-z')^2}{d^4} + \frac{3(z-z')^2}{d^5} - \frac{jk}{d^2} - \frac{k^2(z-z')^2}{d^3} - \frac{1}{d^3}\right] \qquad [11]$$

where

$$d = \sqrt{(z-z')^2 + t^2} \qquad [12]$$

We find the resulting input impedance by taking the integral numerically. We make sure that the number of integration points is at least 10 times larger than l/t.

For optimal SNR performance, the noise resistance, R, should be as small as possible. In Fig. 6, the noise resistance versus antenna length is plotted for two different main field strengths, 1.5 T and 4.7 T. In both cases, R attains a shallow minimum. The antenna length should be chosen around those minima.

From these figures, it is seen that the noise resistance is in the range of 20–30 ohms. Compared to the 0.1–0.5 ohm noise resistance of the catheter coil (Fig. 2), this value is about 50 times larger; therefore, the noise voltage is about seven times larger. However, the signal voltage of the catheter antenna is also larger. The SNR performances of the two sensing devices become equal at a

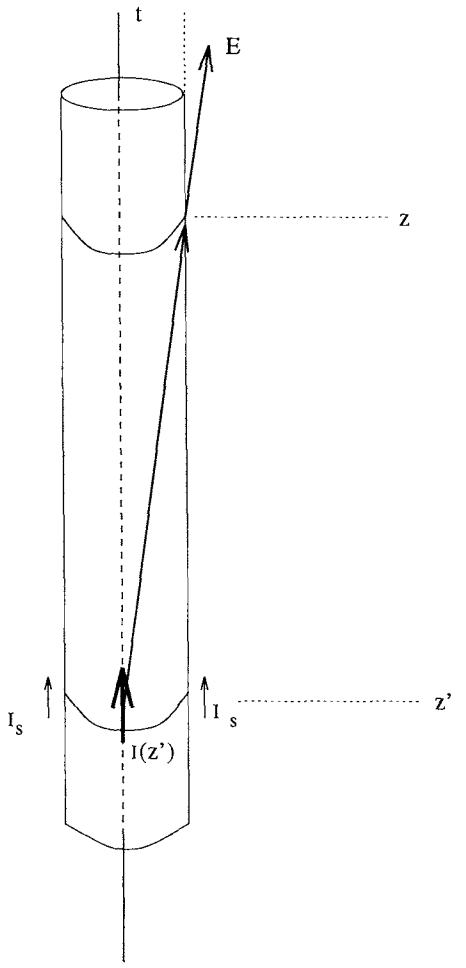

FIG. 5. Geometry for computation of the input impedance. Current at z', passing from the center of the conductor creates an electric field at z on the surface of the conductor.

distance of about 5–8 times the conductor separation for the catheter coil. At smaller distances, the catheter coil has higher SNR, but for larger distances, the catheter antenna has a higher SNR.

To find the signal voltage coming from a voxel, the H field at the spatial location of the voxel is calculated using the formula (15).

$$H = \frac{1}{\mu_0}\nabla \times A \qquad [13]$$

In the very near field of the antenna, the H field varies approximately as $1/r$, but a much better approximation for H can be computed after some symbolic manipulation as,

$$\|H(z, r)\| = r[K(z, r)K^*(z, r)]^{1/2} \qquad [14]$$

where

$$K = \int_{-l}^{l} \frac{f(z')e^{-jkd}}{4\pi}\left[\frac{jk}{r^2 + (z - z')^2} + \frac{1}{(r^2 + (z - z')^2)^{3/2}}\right]dz' \qquad [15]$$

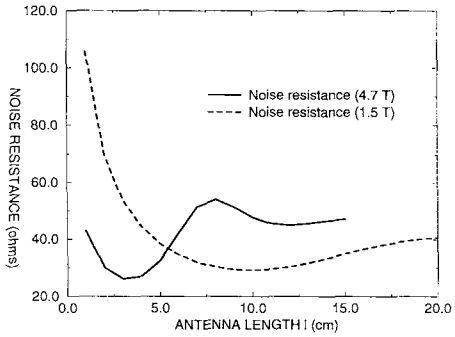

FIG. 6. Noise resistance versus antenna length. Main field 4.7 and 1.5 T, 1 mm thickness, ϵ_r, σ representative of human body tissue.

The numerical calculation of K is relatively straightforward. As a first step in checking our computations, we compared our theoretical results for the input impedance with the previously published curves for finite thickness antennae in lossless media (15) and obtained a very good match. These results justify our omission of the conductor losses, because their contribution to the noise resistance is on the order of a few hundred milliohms.

Using the formulation above, we obtained the sensitivity map of the catheter antenna which is shown in Fig. 7.

Matching, Tuning, and Decoupling Circuitry

The catheter antenna transmits the received signal to the scanner over a coaxial cable. For optimal performance, the input impedance of the catheter antenna must be matched to the characteristic impedance of the coaxial cable. Because the noise resistance of the loopless catheter antenna is large (typically 20–30 ohms), unlike catheter coils (typically 0.1–0.5 ohms), the extra 1–2 ohm noise resistance added by the coaxial cable is acceptable, which makes it possible to place the matching circuit far from the antenna without significant performance degradation.

Similar to the catheter coil, the catheter antenna resonates during RF excitation, which interferes with the flip angle profile and may also create hot spots (points of excessive RF power deposition) inside the body. These can be avoided by electronically damping the resonance of the sensing device during RF excitation. The detuning circuit performs this task by presenting the coaxial cable to the antenna as a very high input impedance port during RF excitation. Various designs are possible to achieve this desired performance. A sample design,

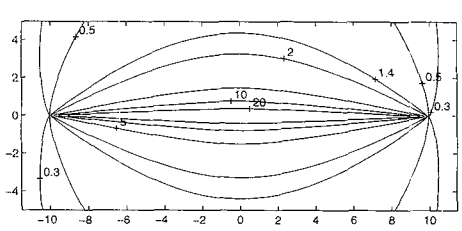

FIG. 7. Sensitivity map of the loopless catheter antenna with arbitrary scaling. X and Y coordinates are in centimeters. The antenna extends from −10 to 10 cm horizontally, in the center of the plot.

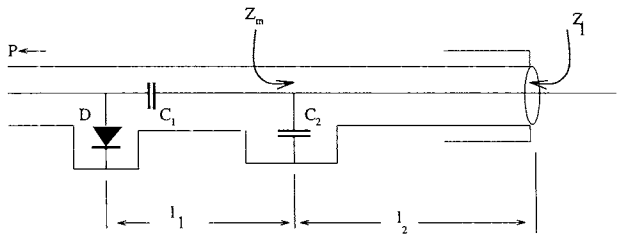

FIG. 8. A, antenna terminal; P, preamplifier; D, pin diode; C_1, DC blocking capacitor; C_2, matching capacitor. l_1, l_2, and C_2 are design parameters. C_1 is a large capacitor.

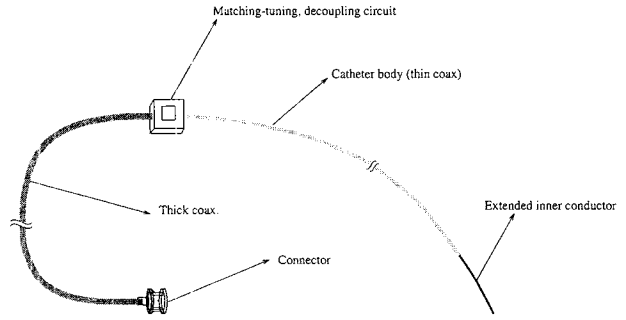

FIG. 9. An illustration of a preliminary design of the catheter antenna. The portion from the tip to the electronic circuitry is inserted into blood vessels.

which was implemented for one of our catheter antennae, is depicted in Fig. 8.

C_2, L_2 is chosen such that $Z_m = Z_0$, the characteristic impedance of the coaxial cable. Then, L_1 is chosen such that when the pin diode is turned on, the impedance, Z_1, seen by the antenna, becomes as high as possible. In our implementation, with tap water as the medium, the values of the design parameters are $C_1 = 500\ pF$; $C_2 = 70\ pF$; $l_1 = 0.06\ \lambda$, $l_2 = 0.209\lambda$; $Z_0 = 50\ \Omega$.

EXPERIMENTAL RESULTS

We designed several catheter antennae and measured their input impedances using a vector impedance meter in saline solution. We then designed and implemented the matching, tuning, and decoupling circuits. A preliminary catheter antenna design is illustrated in Fig. 9.

The performance of the matching circuit is not critical, because the input impedance of the catheter antenna is on the same order as the characteristic impedance of the coaxial cable (50 ohms). We tested the tuning and matching circuit by a reflection meter in saline solution, which has a conductivity similar to mammalian tissue. When the antenna was properly matched and tuned, there was no reflection on the coaxial cable from the antenna terminal at the frequency of operation. Next, we tested the catheter antennae by imaging perforated cardboard in tap water. The phantom images taken by a 9-F catheter coil, a 2.6-F loopless catheter antenna, and the body coil, with identical imaging parameters, are depicted in Fig. 10. The pulse sequences that we used allowed a voxel size of $0.16 \times 0.16 \times 1.5$ mm. These images were acquired with an 8 cm field of view (FOV), 512×512 data acquisition matrix, 2 NEX, and 16 KHz receiver bandwidth. These imaging parameters correspond to an effective pixel bandwidth of 0.06 Hz. We obtained 12 slices of similar images in approximately 10 minutes. As seen from the images, the catheter antenna provides sufficient SNR for the intended image resolution. Observe that the SNR obtained by the catheter coil and the loopless catheter antenna are equal about 1 cm away from the catheters. However, the SNR of the coil is better in the 1-cm area immediately around the center, whereas the SNR of the antenna is higher outside the immediate 1-cm area.

A comparison between theoretical and experimental SNR versus radial distance is depicted in Fig. 11 for a catheter antenna. The experimental values of SNR are computed by dividing pixel values by the noise value estimated from the image. For small values of SNR, this method of computation has a bias (17). The experimental results are in very good agreement with the theory.

The same catheter antenna was inserted from the femoral artery of a rabbit into the aorta using x-ray fluoroscopy. The animal was later moved to the MR suite, and high-resolution axial images of the aortic wall were ob-

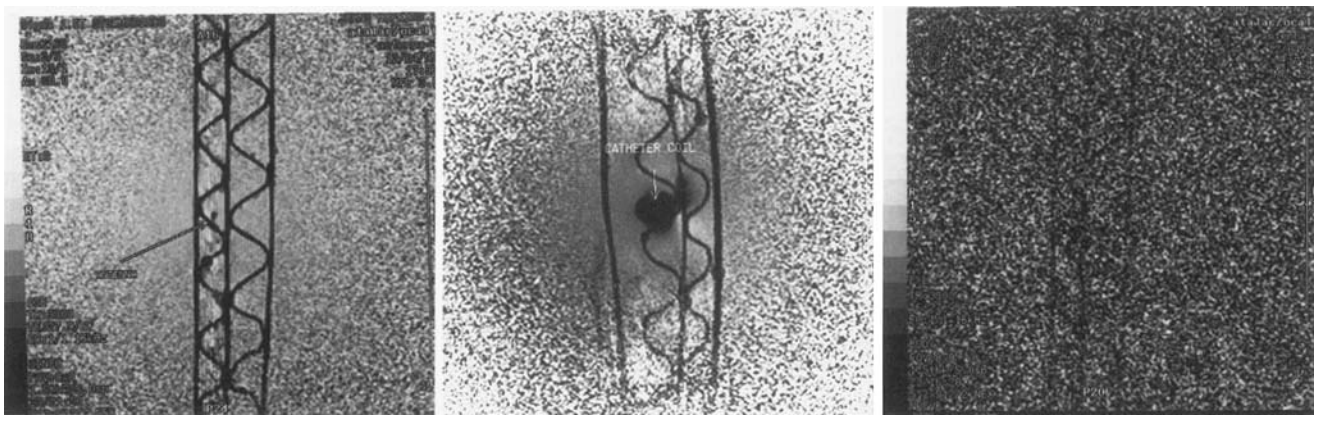

FIG. 10. MR images of a perforated cardboard in tap water: (a) using catheter antenna, (b) catheter coil, (c) using body coil. Imaging parameters for all images are: 8 cm FOV; 512×512 acquisition matrix; 1.5 mm slice thickness; 2 NEX; 16 KHz receiver bandwidth; and TR/TE 3800/27.9. The images (a) and (b) are sensitivity corrected; note the increase in noise with increasing radial distance.

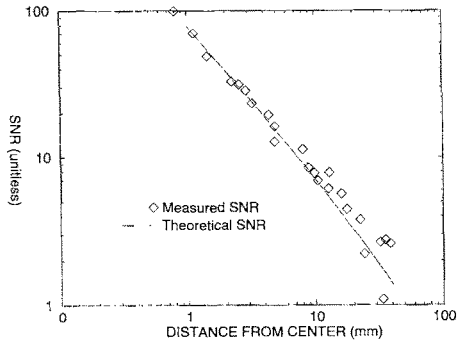

FIG. 11. SNR versus radial distance, a comparison between theory and experiment at 1.5 T. Radial distance is in millimeters. Imaging parameters: 8 cm FOV; 512 × 512 acquisition matrix; 1.5 mm slice thickness; 2 NEX; and 16 KHz receiver bandwidth, which corresponds to voxel size 0.16 × 0.16 × 1.5 mm, 0.06 Hz effective pixel bandwidth.

tained (see Fig. 12). In this image, blood is bright because of the time-of-flight effect, which shows normal blood flow in the aorta. A large FOV image is shown in Fig. 13, to demonstrate the very high sensitivity along the whole length of the catheter. This property of the design can be used for real-time catheter tracking under MR fluoroscopy.

CONCLUSIONS

We designed a catheter antenna, which consisted of a dipole antenna at the tip of a coaxial cable, to increase the SNR in MR imaging of blood vessels. The physical dimensions and flexibility of the catheter antenna make it practical for insertion into blood vessels. The optimal pole length of the antenna at 1.5 T in human tissue is between 7 and 10 cm.

FIG. 12. Rabbit aorta image. Imaging parameters: 4 × 4 cm FOV; 256 × 256 acquisition matrix; 1.5 mm slice thickness; TR/TE 31/6.7; 32 NEX SPGR. A 1 × 1 cm portion of the image is shown.

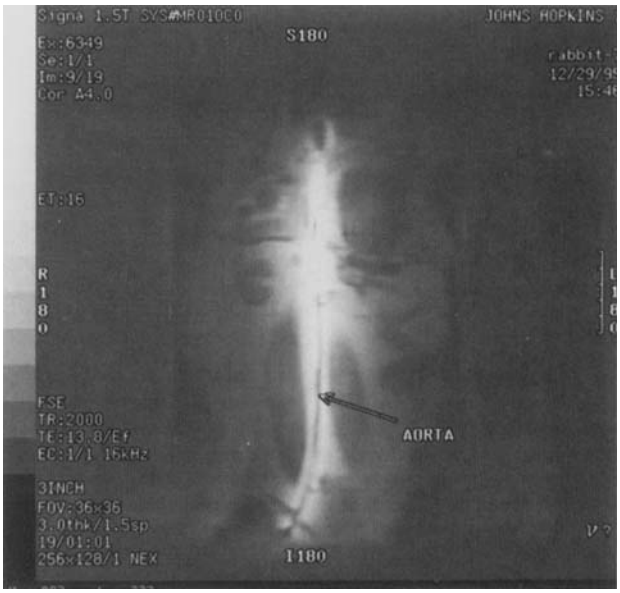

FIG. 13. Large FOV rabbit image, taken with the catheter antenna, without sensitivity correction. To allow peripherals be seen, the brightness around the catheter antenna has been saturated. The dark path in the center corresponds to the aorta. Imaging parameters are: 36 × 36 cm FOV; 256 × 128 data acquisition matrix; 3 mm slice thickness; TR/TE 2000/13.8; and 1 NEX.

It is possible to construct the catheter antenna with a very small diameter. In our electronics laboratory, 1.5-French (0.5 mm) catheter antennae have been produced. A theoretical analysis of the design has been carried out. The theory was then verified with experiments.

The sensitivity of the catheter antenna decays approximately inversely to the radial distance from the center axis. Hence, it provides useful SNR in a cylindrical volume around the catheter. The catheter antenna and catheter coil have similar SNR performances. However, the catheter antenna can be constructed easily in a very thin diameter, and it allows electronic circuits to be placed outside the body.

The catheter antenna has been demonstrated in imaging of phantoms and rabbit aortas *in vivo* with great success. The simple structure of the catheter antenna suggests that this device can be produced and operated reliably and consistently. Further research is required to gather experience in using this device in various interventional techniques.

ACKNOWLEDGMENTS

The authors thank Mary McAllister, Bradley Bolster, and Michael A. Guttman for their help in manuscript preparation.

REFERENCES

1. J. R. Spears, H. J. Marais, J. Serur, O. Pomerantzeff, R. P. Geyer, R. S. Sipzener, R. Weintraub, R. Thurer, In vivo coronary angioscopy. *J. Am. Coll. Cardiol.* **1**, 1311–1314 (1983).
2. B. F. Waller, C. A. Pinkerton, J. D. Slack, Intravascular ultrasound: a histological study of vessel during life. *Circulation* **85**, 2305–2310 (1992).

3. J. D. Pearlman, J. F. Southern, J. L. Ackerman, Nuclear magnetic resonance microscopy of atheroma in human coronary arteries. *Angiology* **42,** 726–733 (1991).
4. M. Asdente, L. Pavesi, P. L. Oreste, A. Colombo, W. Kuhn, E. Tremoli, Evaluation of atherosclerotic lesions using NMR microimaging. *Atherosclerosis* **80,** 243–253 (1990).
5. M. B. Merickel, C. S. Carman, J. R. Brookeman, J. P. Mugler, M. F. Brown, C. R. Ayers, Identification and 3-d quantification of atherosclerosis using magnetic resonance imaging. *Comput. Biol. Med.* **18,** 89–102 (1988).
6. M. B. Merickel, S. Berr, T. R. Jackson, J. Snell, P. Gillies, E. Shimshick, J. Hainer, J. R. Brookeman, C. R. Ayers, Noninvasive quantitative evaluation of atherosclerosis using MRI and image analysis. *Arterioscler. Thromb.* **13,** 1180–1186 (1993).
7. H. L. Kantor, R. W. Briggs, R. S. Balaban, In vivo 31P nuclear magnetic resonance measurements in cacine heart using a catheter-coil. *Circ. Res.* **55,** 261–266 (1984).
8. G. C. Hurst, J. Hua, J. L. Duerk, A. M. Cohen, Intravascular (catheter) NMR receiver probe: preliminary design analysis and application to canine iliofemoral imaging. *Magn. Reson. Med.* **24,** 343–357 (1992).
9. K. Kandarpa, P. Jakab, S. Patz, F. J. Schoen, F. A. Jolesz, Prototype miniature endoluminal mr imaging catheter. *J. Vasc. Interv. Radiol.* **4,** 419–427 (1993).
10. A. J. Martin, D. B. Plewes, R. M. Henkelman, MR imaging of blood vessel with an intravascular coil. *J. Magn. Reson. Imaging* **2,** 421–429 (1992).
11. G. G. McDonald, M. Chwialkowski, R. M. Peshock, Performance comparison of several coil geometries for use in catheters. *Radiology* **189(P)** 319 (1993).
12. A. J. Martin, R. M. Henkelman, Intravascular MR imaging in a porcine animal model. *Magn. Reson. Med.* **32,** 224–229 (1994).
13. E. Atalar, P. A. Bottomley, E. A. Zerhouni, A flexible catheter coil for imaging and spectroscopy of atherosclerotic plaques, *in* "Proc., SMR, 3rd Annual Meeting, Nice, 1995," p. 988.
14. H. Vesselle, R. E. Collin, The signal-to-noise ratio of nuclear magnetic resonance surface coils and application to a lossy dielectric cylinder model—part i: theory. *IEEE Trans. Biomed. Eng.* **42,** 497–506 (1995).
15. S. Ramo, J. R. Whinnery, T. V. Duzer, "Fields and Waves in Communication Electronics," 2nd ed., John Wiley & Sons, New York, 1984.
16. A. Chiabrera, C. Nicolini, H. P. Schwan, "Interactions between Electromagnetic Fields and Cells," NATO, New York, 1985.
17. R. M. Henkelman, Measurement of signal intensities in the presence of noise in MR images. *Med. Phys.* **12,** 232–233 (1985).